COVER SHEET

Synthesis and Characterization of Layered Double Hydroxides with a High Aspect Ratio

Qi Tao[a, b], Yuanming Zhang[a,*], Xiang Zhang[a], Peng Yuan[b], Hongping He[b,*]

[a] *Department of Chemistry, Institute of Nano-Chemistry, Jinan University, Guangzhou, 510632, China*

[b] *Guangzhou Institute of Geochemistry, Chinese Academy of Sciences, Guangzhou 510640, China*

*Corresponding authors. Tel.: 86-20-33334209; fax: 86-20-85226262

E-mail addresses: tzhangym@vip.163.com; hehp@gig.ac.cn

Abstract

A new route for synthesis of Mg/Al layered double hydroxide ($Mg_6Al_2(OH)_{16}(CO_3)\cdot 4H_2O$) has been introduced, which can be considered as a modified calcination-rehydration method. Under the hydrothermal conditions, LDHs with a high aspect ratio were synthesized and characterized by inductively coupled plasma-atom emission spectrometer (ICP-AES), X-ray diffraction (XRD), Fourier transform infrared spectroscopy (FTIR), thermal measurement (TG-DTG) and scanning electron microscopy (SEM). XRD patterns display the crystalline enhanced with the increase of hydrothermal temperature and aging time. TG-DTG curves show the more stable LDHs were synthesized at higher temperature. SEM images indicate the lateral size of the synthesized LDHs locates at ca. 1 - 6 μm and the thickness at ca. 35 - 60 nm. And the particle size depends strongly on the treatment temperature and aging time. A buffer solution consisted of HCO_3^- and CO_3^{2-} keeps the pH of reaction system in a certain range and offers a low supersaturated reaction circumstance. This is of high importance for the formation of LDHs with a high aspect ratio.

***Keywords*:** Layered double hydroxides; Calcination-rehydration method; High aspect ratio; Hydrothermal treatment; Scanning electron microscopy

1. Introduction

Layered double hydroxides (LDHs), also known as hydrotalcite-like compounds or anionic clays, have been investigated as potential materials for adsorbents [1,2], ion-exchangers [3,4], pharmaceutics [5,6], catalysts or catalyst supports [7-9]. The structure of LDHs is similar to that of brucite, $Mg(OH)_2$, and the general formula can be expressed as:

$$[M^{2+}_{1-x} M^{3+}_{x}(OH)_2(A^{n-})_{x/n}] \cdot mH_2O$$

where M^{2+} and M^{3+} are divalent and trivalent cations, respectively. These cations occupy octahedral positions in the hydroxide layer with excessive positive charges. The net positive charge is counterbalanced by the exchangeable interlayer anions, A^{n-}. The stability of the structure is provided by the hydrogen bonds between the hydroxyl groups of octahedral sheets and the intercalated species, anions and water molecules [7].

So far, four different methods have been mainly used to synthesize LDHs, i.e. co-precipitation [10-12], ion-exchange [13,14], calcination-rehydration (reconstruction method) [15-17], and hydrothermal method [18-25]. Ion-exchange method is mainly used for synthesizing LDHs with poly anions [13] or organic anions [14] in the interlayer space. Generally, the LDHs, prepared by the other three routes, contain inorganic anions in the interlayer space.

Co-precipitation method is the most widely used method to synthesize LDHs, in which the mixed alkali soda solution is added to a mixed salt solution and the resultant slurry is aged at a desired temperature. In this case, LDHs always contain a certain amount of CO_3^{2-}, due to the dissolved CO_2 in water and exposure of the resultant slurry in the air, and the particle size is difficult to be controlled [17,20]. However, the abovementioned disadvantages can be overcome when calcination-rehydration method is used. In this case, the property of LDHs, “structure memory effect”, is used to avoid the anionic impurities entering into the interlayer and, to some extent, the distribution of particle size is easy to be controlled [17]. Previous studies [19,21-25] demonstrated that hydrothermal treatments could generally enhance the crystallinity of the resultant LDHs and particle size, which has attracted great interest in the synthesis and application of LDHs. Followed by a hydrothermal treatment with an autogenous vapor pressure, the LDHs prepared from co-precipitation changed its configuration from small patches to big flakes [22]. Miyata [23] reported that the synthesis temperature had a strong effect on crystallite size of LDHs, i.e. crystallite size of LDHs increases with the increase of the temperature from room temperature to 180 °C but decreases above 200 °C. Oh et al. [24] and Kovanda et al. [25] conducted the synthesis experiments under different conditions (e.g. aging time,

reaction temperature and concentrations) to determine the key parameters of affecting the particle size of LDHs. Recently, Xu and co-workers [26] synthesized LDHs with a big lateral dimension (in micrometer scale) and different anions from a mixture of MgO and Al_2O_3 under hydrothermal conditions.

In this work, a modified method was designed to synthesize LDHs on the basis of the three aforementioned methods (co-precipitation, calcination-rehydration and hydrothermal). LDHs with a high aspect ratio (defined as particle diameter/thickness) were synthesized by rehydrolysis of the calcined precursors that were prepared from co-precipitation under hydrothermal conditions. They were characterized by X-ray diffraction (XRD), Fourier transform infrared spectroscopy (FTIR), thermogravimetric measurement (TG), and scanning electron microscopy (SEM). Compared to that reported by Xu and co-workers' [26], the synthesized LDHs display much purer phase and higher aspect ratio. Due to the potential application of such a micrometer scale material as functional coatings and membranes in industry [27,28], it is of high importance to find a general synthesis method to tailor the material morphology and the particle size.

2. Experimental section

2.1 Synthesis and calcination of the original hydrotalcite (MgAl-CO3)

The original hydrotalcites were prepared by co-precipitation as described by Miyata [10]. 38.463 g of $Mg(NO_3)_2{\cdot}6H_2O$ and 18.762 g of $Al(NO_3)_3{\cdot}9H_2O$ with a molar ratio of 2:1 (Mg^{2+}/Al^{3+}) were dissolved in 180 ml deionized water (referred as Solution A). 13.64 g NaOH and 11.31 g Na_2CO_3 were dissolved in 80 ml deioned water (referred as Solution B). At room temperature, Solution B was dropped to Solution A with vigorous stirring, maintaining the pH value of the mixture at ca. 10. The resultant slurry was filtered, washed with deionized water, and dried at 80 °C in an oven.

Calcined sample (marked as S_0) was obtained by calcining MgAl-CO3 in a muffle furnace at 500 °C for 4 h. The calcined product was ground and stored in a desiccator.

2.2 Rehydrolysis of the calcined product under hydrothermal conditions

Rehydrolysis of the calcined product was performed as follows: 0.210 g S_0 and 0.126 g $NaHCO_3$ were added to 20 ml and 60 ml of deionized water, respectively (referred as Series A and Series B). They were dispersed by ultrasonic for 20 min, and the mixture was shifted to an autoclave for a hydrothermal treatment at 110, 140, 160, 180, 200 °C for 12, 24, 36, 48, 72 h, respectively. The samples were marked as $S_{M\text{-}T\text{-}t}$, where M stands for Series A or B, T for reaction temperature and t for

reaction time. All samples were dried at 80 °C in the oven before property analysis. $S_{B\text{-}160\text{-}36}$, for example, presents that sample was prepared at the following reaction condition: 0.210 g S_0 and 0.126 g $NaHCO_3$ were added to 60 ml of deionized water and were shifted to an autoclave for a hydrothermal treatment at 160 °C for 36 h.

2.3 Characterization

Powder X-ray diffraction patterns (XRD) were recorded using a MSML XD-2 instrument (Beijing, China). The Cu Ka (λ = 1.5418, Ni monochromator) radiation was applied at 40 kV and 20 mA with a beam slit DS = SS = 1 mm, RS = 0.30 mm. The samples were measured in the range of 5-75° (2θ) with a speed of 8°/min. Fourier transform infrared (FTIR) spectra were obtained on a Equinox55 infrared spectroscopy (Bruker, Germany) using KBr pellet technique in the range of 400-4000 cm^{-1} with a resolution of 4 cm^{-1}. Thermal gravimetric analyses and differential thermal analyses (TG-DTA) of samples were recorded on a ZRY-2P comprehensive thermobalance (Shanghai, China) at 50-850 °C with a heating ratio of 5 °C/min under air atmosphere. The morphology observation was conducted on a XL-30ESEM scanning electron microscope (Philips, Holland). The compositions of samples were measured by Optima 2000DV ICP-AES (Perkin Elmer Co. America).

3. Results and discussion

3.1 Composition, structure and thermal property

The contents of Mg and Al in the resultant LDHs are shown in Table 1, determined by ICP-AES.

Figure 1 should be paced here.

The molar ratios of Mg^{2+}/Al^{3+} in products are located at 3.00-3.54, similar to that of their precursor, 3.20. This reflects that the rehydrolysis under hydrothermal conditions have little influence on the chemical composition of the resultant LDHs.

The XRD patterns for the samples prepared by co-precipitation and their calcined products are shown in Figure 1. The lack of (003) reflection peak in the calcined product indicates the layered structure of LDHs (Figure 1a) has been destroyed by calcination (Figure 1b) and a phase corresponding to magnesia has formed [23].

Figure 1 should be placed here.

The XRD patterns for LDHs prepared from rehydrolysis under different hydrothermal conditions are shown in Figure 2. The XRD patterns exhibit the characteristic reflections of LDHs with a series of (00l) peaks, which are sharp and symmetric at low 2θ angle, but broad and asymmetric at high 2θ angle. They are characteristic of materials with layered structure [12]. Calculated from the chemical components in Table 1 and the data of TG, the average formula for the resultant hydrotalcite could be expressed as $Mg_6Al_2(OH)_{16}(CO_3)\cdot 4H_2O$.

The hydrothermal treatment results in an increasing intensity of diffraction with the increase of treatment temperature and aged time, particularly for LDHs prepared at 140-180 °C. However, an obvious decrease of the intensity in all three main characteristic peaks, (003), (006) and (009) (see Figure 1) is observed in the diffraction patterns of LDHs prepared at 200 °C (compared with that of 180 °C). At lower temperature and longer reaction time, a spot of metal oxide impurity is found during hydrothermal treatment as shown in Figures 2a and 2d. This is in accordance with the morphology observations (see below).

Figure 2 should be paced here.

The FTIR spectra of all the resultant LDHs are similar. Figure 3 are the spectra of $S_{B\text{-}160\text{-}36}$ (representative of LDHs, Figure 3b) and S_0 (the precursor of the resultant LDHs, Figure 3a). The absorption band around 3500 cm^{-1} is attributed to O-H vibration mode of hydroxyl group and water molecules. Another absorption band corresponding to water deformation is recorded at ca. 1638 cm^{-1}. In addition, there are two weak absorptions in Figure 3b at about 2855 cm^{-1} and 2925 cm^{-1}, which are often found in previous works [10,21,23,30]. The bands less than 850 cm^{-1} are due to the vibration of M-O ($M = Mg^{2+}$, Al^{3+}). The intensities of the bands at 1370 and 670 cm^{-1} of $S_{B\text{-}160\text{-}36}$, corresponding to the vibrations of the interlayer anion (CO_3^{2-}) and M-O, increase when compared to those of S_0. This is due to the decrease of CO_3^{2-} in the interlayer and structural disorder of LDH after calcinations [29, 30]. The absorption at 840 cm^{-1} in both $S_{B\text{-}160\text{-}36}$ and S_0 assigned to the out plane vibration of CO_3^{2-} [30] becomes stronger and wider. After calcination, the brucite-type layers of LDHs are destroyed mostly and the force to obstruct the out plane vibration of CO_3^{2-} residue becomes much weak than before calcination.

Figure 3 should be placed here.

The TG-DTG curves of representative samples are shown in Figure 4. The results of the thermogravimetric analyses are summarized in Table 2. The mass losses of LDHs start at room temperature and complete at around 450 °C. Theoretically, three major mass losses should be

observed. Unfortunately, in this study, only the LDHs prepared at higher temperature display these three corresponding peaks (Figures 4e and 4f). The others (Figures 4a-4d) only show two major mass losses. For $S_{A\text{-}110\text{-}12}$ (Figure 4a), the first loss begins at room temperature and ends at 188.6 °C, corresponding to the loss of the adsorbed water and the interlayer water. The total mass loss in this step is 17.53%. The second step ends at 398.0 °C with a mass loss of 33.89%, attributed to the dehydroxylation and decomposition of the interlayer anions. The splitting doublet DTG peaks at higher temperature implies the strong interaction between the interlayer anions and the backbone. Figures 4b-4d show similar thermal character of the corresponding samples. Their first loss happens at 202.5-219.1 °C with mass losses of 21.93-25.20%. The second loss step takes place at 375-402 °C with mass losses of 21.93-25.20%. The samples synthesized at higher temperature (Figures 4e and 4f) give three mass losses clearly. This suggests that the LDHs obtained at higher temperature present better thermal stability than those synthesized at lower temperatures with shorter time. The difference between them is that the mass loss of $S_{B\text{-}180\text{-}60}$ is always larger than that of $S_{B\text{-}200\text{-}72}$. Yun and Pinnavaia [31] reported that the desorption temperature of LDH for complete removal of the surface-bound water increased with increasing Al content. However, this phenomenon has not been observed in this study. The present study indicates that the higher Al content results in a larger amount of mass loss. The most likely interpretation is that the higher Al content (Table 1) gives higher layer charge density, which offers more combined hydroxyls, water molecules and carbonates. And these water molecules adsorbed on the surface of LDHs give a small mass loss of 3.21% and 2.55% as found in $S_{B\text{-}180\text{-}60}$ and $S_{B\text{-}200\text{-}72}$. This suggestion can be evidenced by the analogous of $S_{A\text{-}110\text{-}12}$.

Figure 4 should be placed here.

Table 2 should be paced here.

3.2 Morphology

The SEM images of the samples prepared under different conditions are shown in Figure 5. From the SEM images, it can be seen that, at lower temperature and less aged time, the LDHs show small patches with some amorphous conglomeration (the metallic oxide impurities, which have been proved by the XRD, Figures 5a and 5b). The patches grow with the increase of time and temperature (Figure 5c). Finally, when reaction temperature rises to 160 °C or 180 °C and the reaction time is prolonged to 48 h, large and thin sheets become prevalent (Figures 5d and 5e). At these temperatures, prolong the

reaction time, only to cause decrease in particle size and amorphous form or impure in phase. When temperature reaches 200 °C, more amorphous impurities appear and the size of sheets seems not to enlarge any more. The lateral dimension increases from about 0.5 μm to 6.0 μm, which is larger than that reported by Xu and the co-workers [26]. Estimated from the SEM images, the lateral thickness is between 35 and 60 nm. The sheet-like LDHs with such a high aspect ratio is beyond what was previously reported [21,26,32].

Figure 5 Should be placed here.

3.3 Crystal growth mechanism

The comparatively large particle size of the resultant LDHs in this study can be explained as follows: Firstly, the synthesis reaction is conducted under the hydrothermal conditions. In this case, high pressure restricts the growth direction (c axis direction) for new-formed crystallites [32]; crystal growth comes to the other two directions. Secondly, the HCO_3^- is adopted to provide the appropriate concentration of CO_3^{2-}. In this reaction system, there are two ionization equilibriums including HCO_3^- and H_2O in alkalescent condition. The reactions are as follows:

$$\mathbf{M^{2+}_{1-x}M^{3+}_{x}O_{1+x/2}} + \mathit{(x/2)}\ \mathrm{H}\mathbf{CO_3^-} + \mathit{(1 - x/2 + m)}\ \mathbf{H_2O} \longrightarrow \mathbf{M^{2+}_{1-x}M^{3+}_{x}(OH)_2\ (CO_3)_{x/2}} \cdot \mathit{m}\ \mathbf{H_2O} + \mathit{x/2}\ \mathbf{OH^-} \quad (1)$$

When superfluous HCO_3^- is considered, the whole reaction may be replaced as the Eq. (2)

$$\mathbf{M^{2+}_{1-x}M^{3+}_{x}O_{1+x/2}} + \mathit{x}\ \mathbf{HCO_3^-} + \mathit{(1 - x/2 + m)}\ \mathbf{H_2O} \longrightarrow \mathbf{M^{2+}_{1-x}M^{3+}_{x}(OH)_2\ (CO_3)_{x/2}} \cdot \mathit{m}\mathbf{H_2O} + \mathit{x/2}\ \mathbf{CO_3^{2-}} \quad (2)$$

A buffer solution was formed with the CO_3^{2-} and HCO_3^- anions, even MgAl-CO3 produced in the system. The buffer ion pair prevents the pH value change of reaction system. The pH of the solutions before and after the reaction were measured and the values are located at 10 – 9 (Series A) and 9 - 8 (Series B), respectively. This pH range is suitable for forming of hydrotalcite phase and supports our suggestion about the formation mechanism of hydrotalcite. Furthermore, the buffer ion pair offers a low supersaturated solution during forming the LDHs. Oh and co-workers [24] adopted urea as a source of interlayer anion and alkalescent condition. They suggested that the formation of crystal nuclei or nucleation could be considered as a process, which determines the size of the product

crystals and the nucleation rate increases uniformly with increasing supersaturation ratio. Consequently, the low degree of supersaturation ratio results in the decrease of nucleation rate, and lead to a larger crystal size.

At high temperature, the LDHs show rounded hexagonal shape, indicating signs of dissolution during hydrothermal treatment [21]. So it could be believed that metal oxides are dissolved and the carbonates intercalate into the interlayer space of LDHs, and subsequently, re-crystallization happens [18]. On the other hand, some smaller particles without certain figure can be found concomitant with the predominant big sheets. Kloprogge [21] proposed that the smaller particles were the initial growth stage of the phase that is composed of Mg and O with a ratio of 1:1. The presence of these patches indicates that predominant crystal growth occurs on the edges with an increase of aging time, resulting in relatively thin hexagonal plate-shaped crystals with rounded edges. Consequently, the crystal particle size grows bigger and bigger, and the shape become more and more regular. Combined with the results of XRD patterns, SEM images and TG-DTG, we may conclude that LDHs with higher aspect ratio, high crystallinity and better thermal stability are formed at 160-180 °C with a reaction time of 48 h.

4. Conclusions

LDHs with a high aspect ratio are synthesized via a modified calcinations-rehydration process. The particle size can be tailored by changing the parameters of hydrothermal treatments. The aspect ratio of LDHs synthesized in this study is higher than those reported in the literature. Under suitable conditions, the resultant material shows higher purity than the precursors, and the Mg^{2+}/Al^{3+} molar ratios are close to the “raw material”. The crystal growth depends on the buffer system to hold the pH value and to keep the reaction solution at low supersaturated. The latter is prior factor in controling the crystal growth. The crystalline resultants with higher aspect ratio and better thermal stability were synthesized at 160-180 °C with reaction time of 48 h.

References

[1] M.C. Hermosín, I.Pavlovic, M.A. Ulibarri, J. Cornejo, Water Res. 30 (1996) 171.
[2] N.D. Hutson, S.A. Speakman, E.A. Payzant, Chem. Mater. 16 (2004) 4135.
[3] E.D. Dimotakis, T.J. Pinnavaia, Inorg. Chem. 29 (1990) 2393.
[4] Y.W. You, H.T. Zhao, G.F. Vance, J Mater. Chem. 12 (2002) 907.
[5] S.H. Hwang, Y.S. Han, J.H. Choy, B. Kor. Chem. Soc. 22 (2001) 1019.
[6] Z.L. Wang, E.B. Wang, L.Gao, L.Xu, J. Solid State Chem. 178 (2005) 736.

[7] F. Cavani, F. Trifiro, A. Vaccari, Catal. Today 11 (1991) 173.
[8] B.M. Choudary, N.S. Chowdari, K. Jyothi, M.L. Kantam, J. Am. Chem. Soc. 124 (2002) 5341.
[9] K. Motokura, D. Nishimura, K. Mori, T. Mizugaki, K. Ebitani, K. Kaneda, J. Am. Chem. Soc. 126 (2004) 5662.
[10] S. Miyata, Clays Clay Miner. 23 (1975) 369.
[11] M.A. Aramendía, V. Borau, C. Jiménez, J.M. Marinas, J.R. Ruiz, F.J. Urbano, J. Solid State Chem. 168 (2002) 156.
[12] V.R.L. Constantino, T.J. Pinnavaia, Inorg. Chem. 34 (1995) 883.
[13] M.A. Ulibarri, F.M. Labajos, Inorg. Chem. 33 (1994) 2592.
[14] S. Aisawa, Y. Ohnuma, K. Hirose, S. Takahashi, H. Hirahara, E. Narita, Appl. Clay Sci. 28 (2005) 137.
[15] K. Chibwe, W. Jones, J. Chem. Soc. Chem. Commun. 14 (1989) 926.
[16] E. Narita, P. Kaviratra, T.J. Pinnavaia, Chem. Lett. 20 (1991) 805.
[17] T. Hibino, A. Tsunashima, Chem. Mater, 10 (1998) 4055.
[18] M. Ogawa, S. Asai. Chem. Mater, 12 (2000) 3253.
[19]G.T. Chandrappa, N. Steunou, S. Cassaignon, C. Bauvais, J. Livage, Catal. Today 78 (2003) 85.
[20] S. Möhmel, I. Kurzawski, D. Uecker, D. Müller, W. Gessner, Crystal. Res. Tech. 37 (2002) 359.
[21] J.T. Kloprogge, L. Hickey, R.L. Frost, J. Solid State Chem. 177 (2004) 4047.
[22] F.M.Labajos, V. Rives, M.A. Ulibarri, J. Mater. Sci. 27 (1992) 1546.
[23] S. Miyata, Clay. Clay Miner. 28 (1980) 50.
[24] J.M. Oh, S. H. Hwang, J.H. Choy, Solid State Ionics 151 (2002) 285.
[25] F. Kovanda, D. Kolousek, Z. Cilova, V. Hulinsky, Appl. Clay Sci. 28 (2005) 101.
[26] Z.P. Xu, G..Q. Lu, Chem. Mater. 17 (2005) 1055.
[27] E. Gardner, K.M. Huntoon, T.J. Pinnavaia, Adv. Mater. 13 (2001) 1263.
[28] T. Kimura, Y. Tokura, Ann. Rev. Mater. Sci. 30 (2000) 451.
[29] W. Yang, Y. Kim, P.K.T. Liu, M. Sahimi, T.T. Tsotsis, Chem. Eng. Sci. 57 (2002) 2945.
[30] L. Hickey, J.T. Kloprogge, R.L. Frost, J. Mater. Sci. 35 (2000) 4347.
[31] S.K. Yun, T.J. Pinnavaia, Chem. Mater. 7 (1995) 348.
[32] Y. Zhao, F. Li, R. Zhang, D.G. Evans, X. Duan, Chem. Mater. 14 (2002) 4286.

Table 1. Properties of the samples selected

Sample	Mg / wt%	Al / wt%	The molar ratios of Mg^{2+}/Al^{3+}	d_{003} / nm	Intensity of d_{003} /Cps
S_0	22.17	7.70	3.20	—	—
$S_{A\text{-}110\text{-}12}$	23.60	7.40	3.54	0.793	2373
$S_{B\text{-}110\text{-}12}$	24.34	8.92	3.03	0.787	2465
$S_{B\text{-}140\text{-}24}$	21.43	7.61	3.13	0.785	3667
$S_{B\text{-}160\text{-}36}$	28.24	10.45	3.00	0.776	5709
$S_{B\text{-}180\text{-}48}$	37.88	13.45	3.13	0.782	7574
$S_{B\text{-}200\text{-}72}$	27.28	9.33	3.25	0.783	6267

Table 2. Results of Mass Losses of the TG-DTG for the Selected Samples

	Step 1		Step 2		Step 3		
	Mass loss %	**Temp. /°C**	**Mass loss %**	**Temp. /°C**	**Mass loss %**	**Temp. /°C**	**Total mass loss %**
$S_{A\text{-}110\text{-}12}$	17.53	188.6	33.89	398.0	—	—	51.42
$S_{B\text{-}110\text{-}12}$	15.43	202.5	23.35	398.0	—	—	38.78
$S_{B\text{-}140\text{-}24}$	14.18	219.1	21.93	402.4	—	—	36.11
$S_{B\text{-}160\text{-}36}$	13.60	214.2	25.20	375.9	—	—	38.80
$S_{B\text{-}180\text{-}48}$	3.21	149.1	9.56	231.3	25.16	428.4	37.93
$S_{B\text{-}200\text{-}72}$	2.55	106.5	17.72	211.4	24.56	400.1	44.83

Figure Captions

Figure 1. The XRD patterns of LDHs synthesized by co-precipitation (a) and its calcined resultant (b, S_0).

Figure 2. The XRD patterns of LDHs prepared via rehydration under hydrothermal condition. (a) $S_{A\text{-}110\text{-}t}$, (b) $S_{B\text{-}110\text{-}t}$, (c) $S_{B\text{-}T\text{-}36}$, (d) $S_{B\text{-}T\text{-}72}$.

□ represents the metal-oxides impurity.

Figure 3. The FTIR of representative LDHs samples prepared via rehydration under hydrothermal condition and its calcined precursor. (a) S_0, (b) $S_{B\text{-}160\text{-}36}$.

Figure 4. The TG/DTA of selected LDHs samples prepared via rehydration under hydrothermal condition. (a) $S_{A\text{-}110\text{-}12}$, (b) $S_{B\text{-}110\text{-}12}$, (c) $S_{B\text{-}140\text{--}24}$, (d) $S_{B\text{-}160\text{-}36}$, (e) $S_{B\text{-}180\text{-}48}$, (f) $S_{B\text{-}200\text{-}72}$.

Figure 5. The SEM of the samples obtained from different hydrothermal conditions. (a) $S_{A\text{-}110\text{-}12}$, (b) $S_{B\text{-}110\text{-}36}$, (c) $S_{B\text{-}140\text{-}48}$, (d) $S_{B\text{-}160\text{-}36}$, (e) $S_{B\text{-}160\text{-}48}$, (f) $S_{B\text{-}160\text{-}72}$, (g) $S_{B\text{-}180\text{-}48}$, (h) $S_{B\text{-}180\text{-}72}$, (i) $S_{B\text{-}200\text{-}72}$.

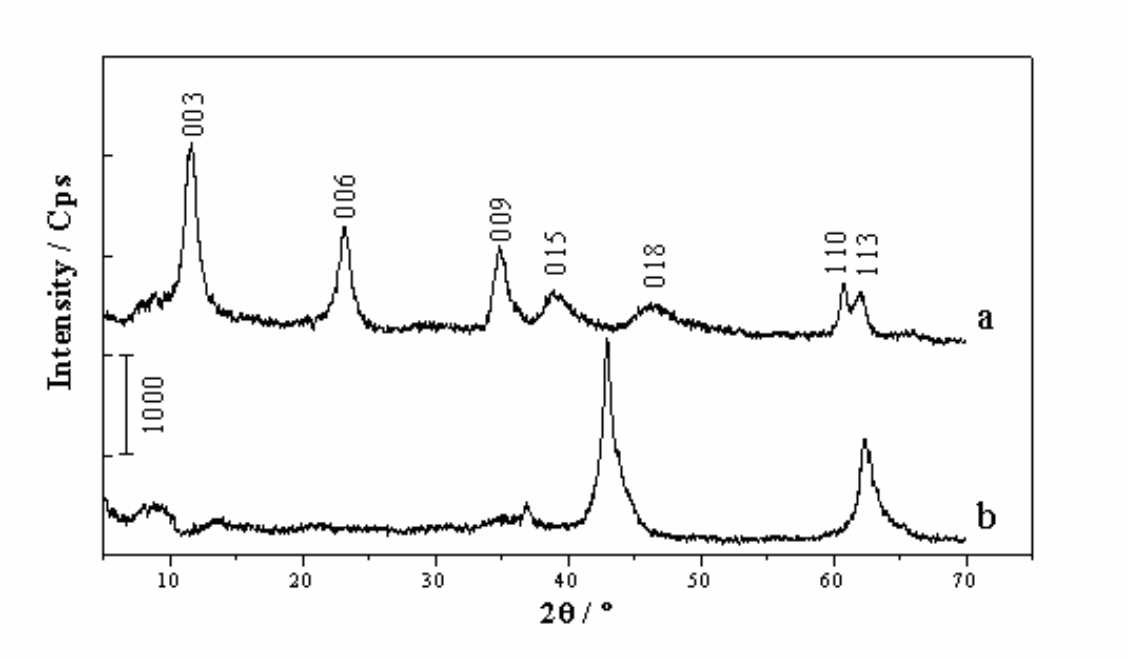
Intensity / Cps
003
006
009
015
018
110
113
a
1000
b
10
20
30
40
50
60
70
2θ / °

Figure 1

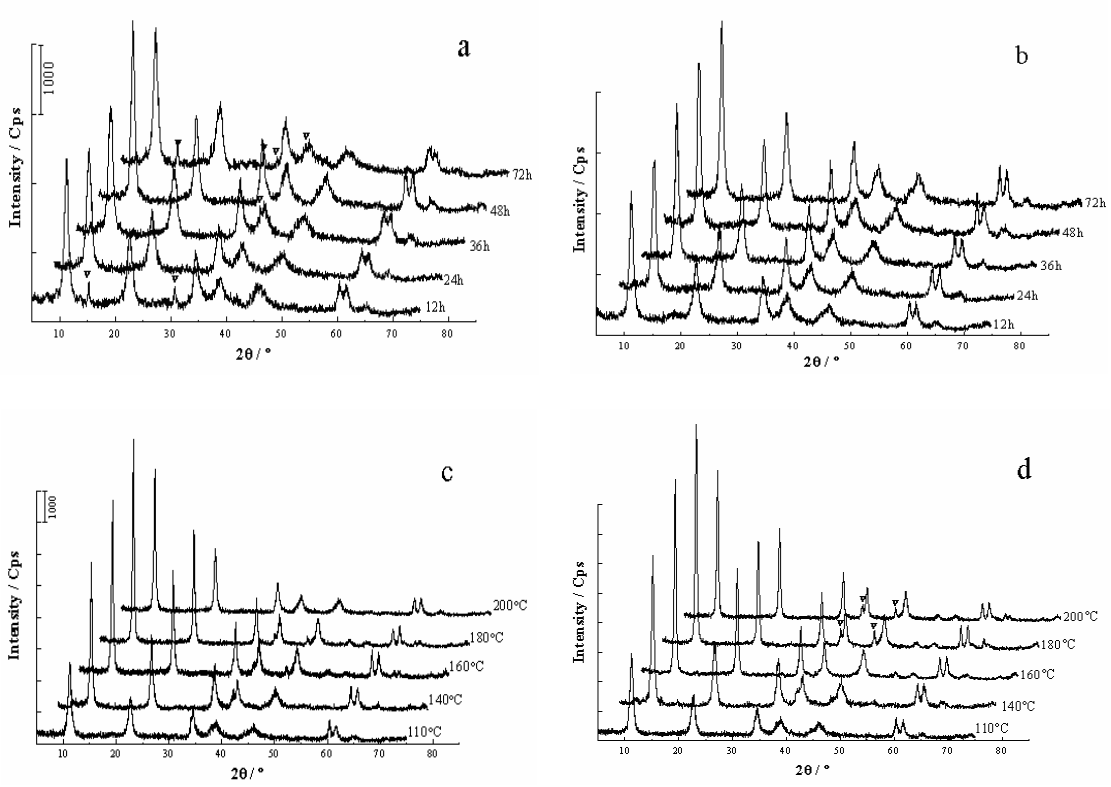
a
1000
Intensity / Cps
72h
48h
36h
24h
12h
2θ / °
b
Intensity / Cps
72h
48h
36h
24h
12h
2θ / °
c
1000
Intensity / Cps
200°C
180°C
160°C
140°C
110°C
2θ / °
d
Intensity / Cps
200°C
180°C
160°C
140°C
110°C
2θ / °

Figure 2

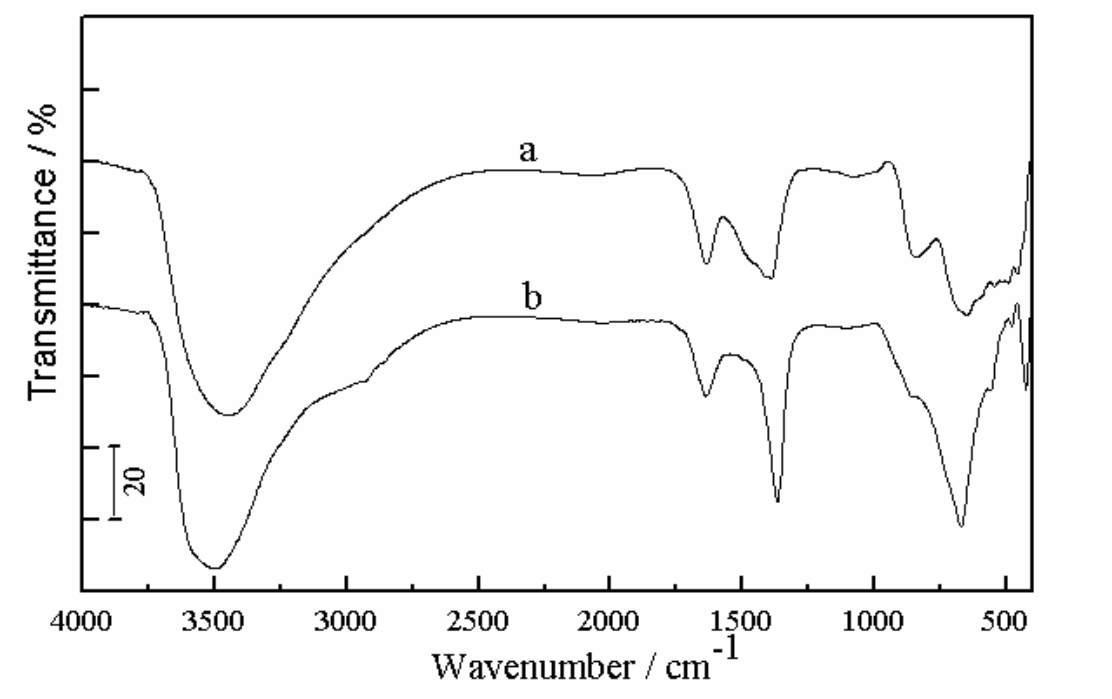
Transmittance / %
a
b
20
4000
3500
3000
2500
2000
1500
1000
500
Wavenumber / cm-1

Figure 3

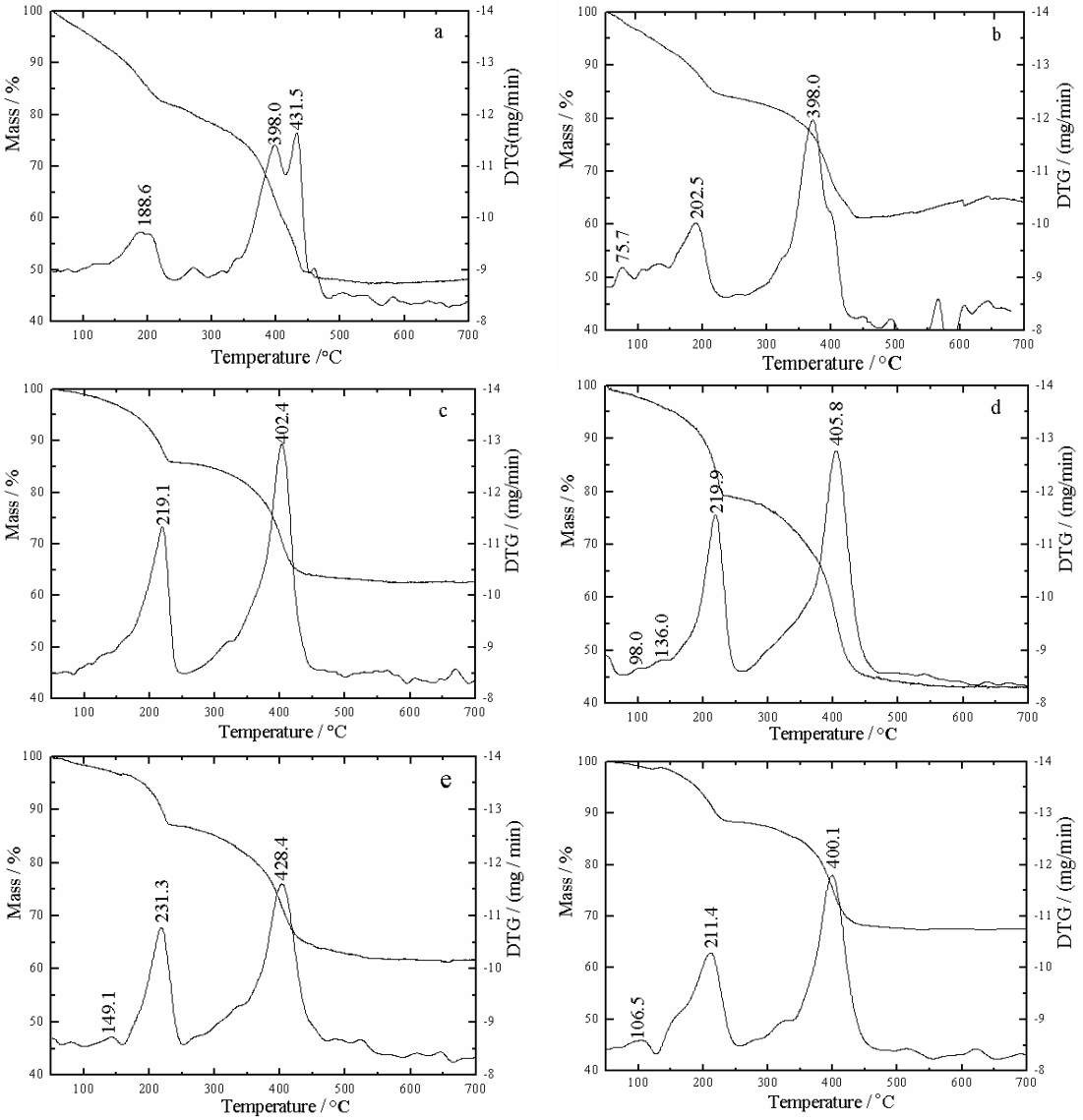
a
Mass / %
DTG(mg/min)
Temperature /°C
188.6
398.0
431.5
b
Mass / %
DTG / (mg/min)
Temperature / °C
75.7
202.5
398.0
c
Mass / %
DTG / (mg/min)
Temperature / °C
219.1
402.4
d
Mass / %
DTG / (mg/min)
Temperature / °C
98.0
136.0
219.9
405.8
e
Mass / %
DTG / (mg / min)
Temperature / °C
149.1
231.3
428.4
Mass / %
DTG / (mg/min)
Temperature / °C
106.5
211.4
400.1

Figure 4

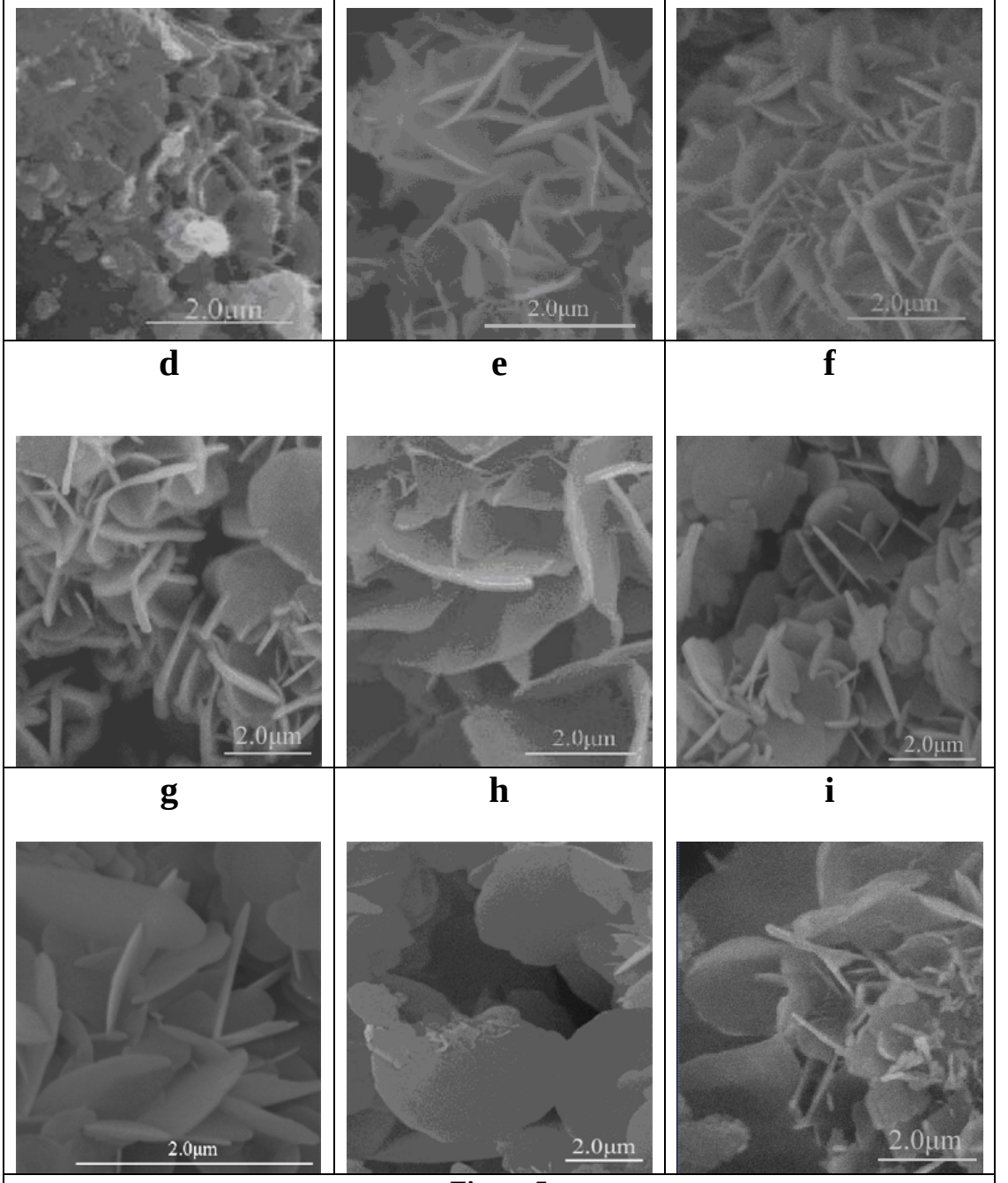

Figure 5